THE JOURNAL OF PHYSICAL CHEMISTRY C

Article

pubs.acs.org/JPCC

Surface Chemistry of 4-Mercaptobenzoic Acid Self-Assembled on Ag(111) and Ag Nanoparticles

Julie V. Maya Girón,[†] Eugenia Zelaya,[‡] Aldo Rubert,[†] Guillermo Benítez,[†] Pilar Carro,[§] Roberto C. Salvarezza,[†] and Maria E. Vela*[,†]

[†]Instituto de Investigaciones Fisicoquímicas Teóricas y Aplicadas (INIFTA) Facultad de Ciencias Exactas, Universidad Nacional de La Plata, CONICET Sucursal 4 Casilla de Correo 16, (1900) La Plata, Argentina

[‡]CAB-CNEA, CONICET, Av. Bustillo km 9.5 (R8402AGP), S.C. de Bariloche, Argentina

[§]Departamento de Química Física, Instituto de Materiales y Nanotecnología, Universidad de La Laguna, Tenerife, Spain

Supporting Information

ABSTRACT: The adsorption of 4-mercaptobenzoic acid (MBA) on Ag(111) and Ag nanoparticles (AgNPs) has been studied by X-ray photoelectron spectroscopy (XPS), electrochemical techniques, high-resolution transmission electron microscopy (HRTEM), and density functional theory (DFT) calculations. Results show that MBA molecules adsorb intact on the Ag (111) surface via a thiolate bond, arranged in a $(\sqrt{3} \times 4)$ lattice with coverage $\theta = 0.25$. The phase diagram built using DFT data shows that this lattice is more stable than the dense $(\sqrt{7} \times \sqrt{7})R19.1°$ MBA lattices on reconstructed Ag(111) surfaces. No significant amounts of sulfide were found neither on the Ag(111) surfaces nor on MBA-protected AgNPs, suggesting that the Ag core@Ag-sulfide shell structure where thiolates could be grafted cannot be applied to the MBA-protected AgNPs. Slow degradation of the MBA protective layer in ambient conditions on the AgNPs results in disulfide formation and AgNP sintering.

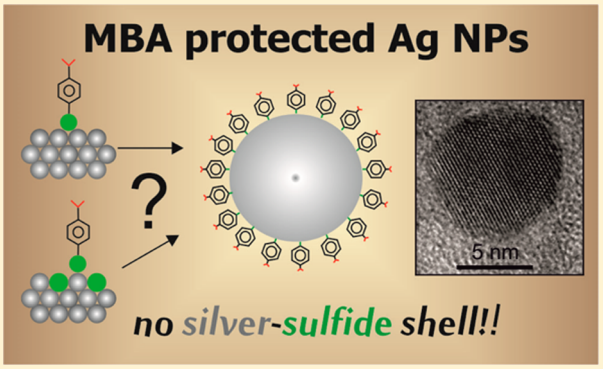

INTRODUCTION

Self-assembled monolayers (SAMs) of thiols on Au and Ag have attracted considerable attention in the past 25 years due to their multiple applications in nanoscience and nanotechnology.[1−5] Previous works have shown that thiols adsorb on Ag(111) as thiolates forming at saturation coverage a distorted $(\sqrt{7} \times \sqrt{7})R19.1°$ lattice with $\theta \approx 0.44$. The molecules adopt a standing-up configuration with a tilt angle between $\alpha \approx 0-19°$.[6,7] On the other hand, experimental data from different techniques indicate that the strong thiol adsorption induces a reconstruction of the Ag(111) surface.[8] The first model, proposed for methanethiol (MT) on the reconstructed Ag(111) surface (R), involves a near-hexagonal surface layer with a Ag density that is only 3/7 of the underlying substrate layers and with the organic molecules adsorbed into 3-fold coordinated hollow sites.[9] This arrangement is also consistent with the observed $(\sqrt{7} \times \sqrt{7})R19.1°$ lattice (nearest-neighbor distance $d = 0.44$ nm) although the substrate has been strongly reconstructed by vacancies formation. Later, it was shown that this model does not imply a better thermodynamic stability since it has a similar surface free energy value (γ) to that estimated for the $(\sqrt{7} \times \sqrt{7})R19.1°$ MT lattice on the unreconstructed (U) surface. It is not surprising because the formation of 4/7 Ag vacancies implies a large energy cost.[10] More recently, a new surface structure has been proposed for MT on the Ag(111) surface with better stability as it involves a greater density (5/7) of topmost Ag atoms; i.e., the vacancy number (and the energy cost) has been reduced.[11] In this case the adsorption pattern consists in $Ag_3(MT)_3$ units surrounded by hexagons of Ag atoms. On the other hand, for longer alkanethiols than MT, the same reconstructed model seems to be valid, although d increases to ≈0.47 nm in order to optimize hydrocarbon chain interactions.[8,12,13] Finally, it has been reported that thiols adsorb intact on Ag(111)[14] although exposure to UV radiation[15] or thermal desorption at high temperature[14] causes C−S bond scission and the formation of S-rich Ag surfaces.

The surface chemistry seems to be more complex in the case of thiolate-protected Ag nanoclusters (AgNC) and nanoparticles.[16] In fact, the structure of 2 nm size AgNPs prepared by reduction of $Ag(SCH_2CH_2Ph)$ precursor has been described as a core−shell structure model with a 92-atom Ag core and an encapsulating protective shell containing Ag atoms and 60 thiolates arranged in a network of six-membered rings resembling the geometry found in alkanethiolate SAMs on the reconstructed Ag(111); i.e., a correlation between thiol

Received: October 2, 2013
Revised: October 28, 2013

   dx.doi.org/10.1021/jp409785c | J. Phys. Chem. C XXXX, XXX, XXX−XXX

organization on the Ag(111) and AgNC surface is proposed.[17] On the other hand, DFT calculations for small $Ag_m(SCH_3)_n$ clusters have shown that -RS-Ag-RS- complexes (RS = thiolate) could be the stable species on the Ag surface[18] as has been observed on Au nanoclusters.[19] A significant contribution recently published has shown that $Ag_{44}(MBA)_{30}$ (MBA = 4-mercaptobenzoic acid) nanoclusters are protected by six $Ag_2(MBA)_5$ units in which Ag cations bind to three thiolate ligands in a planar $Ag(MBA)_3$ configuration.[20] The presence of these species was also confirmed for fluorinated arylthiols on the same clusters.[21] Therefore, particles smaller than 2 nm seem to exhibit complex surface structures that cannot be easily correlated with the experimental data for thiol arrangement on the planar Ag(111) surfaces. Finally, experimental results for dodecanethiolate-protected AgNPs have been consistent with a core−shell structure consisting in a metallic Ag core surrounded by a Ag_2S-like phase.[22] Similar core−shell structure has been found for thiolate-protected AgNPs prepared from the allylmercaptan adsorption.[23] Thus, in these cases thiolates seem to be grafted to a sulfide-covered AgNPs surface, a model that closely resembles that described for thiolate-protected PdNPs.[24] Therefore, the understanding of the surface chemistry and structure of AgNPs deserves special attention.

Thus, the control of the surface chemistry of thiol-capped Ag nanoparticles constitutes an important point regarding the multiple applications in which they are involved. Aromatic thiols on Ag[20,21] have promising applications as key elements for electronic devices[25,26] and SERS-active systems.[27−30] In particular, SAMs of MBA on Ag surfaces are particularly attractive. In fact, the possibility to change the charge of the carboxylate group controlling the pH solution converts this molecule as an efficient anchor for cationic species.[31−34] The presence of the aromatic system in the MBA molecules favors electron transport and charge transfer processes, properties which are relevant in molecular-based electronic and electrochemical devices. Also, MBA-protected Au or Ag NPs are water-soluble, allowing different applications in biological systems. In this context, a detailed knowledge of the surface chemistry and structure of MBA-protected AgNPs is crucial considering the formation of a silver sulfide shell on the metallic core recently reported for thiol self-assembly on AgNP surfaces.[22,23]

In this work we have performed an experimental study of MBA adsorption on the Ag(111) surface and AgNPs in order to clarify the surface chemistry of these systems. DFT calculations are also presented to explore the different plausible models for MBA adsorption on the Ag surfaces.

EXPERIMENTAL SECTION

Materials. 4-Mercaptobenzoic acid (MBA) (Sigma-Aldrich, 90%), NaOH (Sigma-Aldrich, 98.6%), 1-hexadecanethiol (Sigma-Aldrich, 99%), 1-hexanethiol (Sigma-Aldrich, 99%), Ag_2SO_4 (Merck, pro-analysis), H_2SO_4 (Carlo Erba, 98%), and absolute ethanol (Carlo Erba, 99.5%) were used as received. The Ag(111) substrates were prepared in the following way. Evaporated Au films on glass with (111) preferred orientation (Arrandee, Germany) were used as platforms. After annealing for 3 min with a hydrogen flame, these Au substrates exhibit atomically smooth (111) terraces separated by steps of monatomic height, as revealed by scanning tunneling microscopy (STM). Then, Ag (1 × 1)-Au(111) surfaces (hereafter Ag-upd substrates) were voltammetrically prepared by underpotential deposition of Ag on the Au substrate from 5 × 10^{-4} M Ag_2SO_4 + 1 M H_2SO_4 at a scan rate of ν = 0.01 V s^{-1} in the range 0.030−0.65 V. The 0.030 V cathodic limit was used to ensure a coverage between 1 and 2 Ag monolayers (Figure S1, Supporting Information). The voltammetric runs were made in a glass-made electrochemical cell containing three electrodes. A large Pt plate was used as a counterelectrode and an Ag wire as reference. In some experiments polycrystalline Ag foils (∼99.99%) were chemically etched with a mixture 1:1 of 100 vol H_2O_2 and ammonia solution 25% (GR for analysis) for 3 min. They were copiously washed with Milli-Q water and immediately immersed in the MBA solution.

Self-Assembly of Thiols on Planar Surfaces. The MBA SAMs were prepared on Ag-upd substrates or on etched Ag foils by immersion of the clean substrates in 1 mM MBA + 0.1 M NaOH solutions for 1 h 30 min. The possible effect of the solvent on the MBA SAMs coverage was checked by also performing the self-assembly in 1 mM MBA ethanolic solution for the same immersion time. We also verified that longer immersion times (24 h) do not change thiol coverage and chemical composition of the SAM. Hexanethiol (C6) and hexadecanethiol (C16) SAMs were prepared by incubation of freshly prepared Ag-upd substrates in 1 mM ethanolic solution of these thiols for 24 h. Sulfide adsorption was performed dipping silver foil substrates in 1 mM sodium sulfide aqueous solutions for 5 min. Afterward, thiol-protected or sulfide-covered Ag substrates were placed in the UHV chamber for X-ray photoelectron spectroscopy (XPS) analysis or in a conventional glass cell containing 0.1 M NaOH aqueous solution for electrochemical characterization.

X-ray Photoelectron Spectroscopy. X-ray photoelectron spectroscopy (XPS) was performed using a Mg Kα source (XR50, Specs GmbH) and a hemispherical electron energy analyzer (PHOIBOS 100, Specs GmbH). A two-point calibration of the energy scale was performed using sputtered cleaned gold (Au $4f_{7/2}$, binding energy (BE) 84.00 eV) and copper (Cu $2p_{3/2}$, BE: 932.67 eV) samples.

For spectra deconvolution of the S 2p and Ag 3d region, a Shirley type background was subtracted, and a combination of Lorentianz and Gaussian functions was used. In the case of S 2p, the full width at half-maximum (fwhm) was fixed at 1.1 eV. The S $2p_{3/2}$−S $2p_{1/2}$ and Ag $3d_{5/2}$−Ag $3d_{3/2}$ doublets were fitted by using the same fwhm for the two spin−orbit components of the same signal, with spin orbit splitting of 1.2 eV for S 2p and 6.0 eV for Ag 3d and branching ratios S $2p_{3/2}$/S$2p_{1/2}$ = 2 and Ag $3d_{5/2}$/Ag $3d_{3/2}$ = 3/2, respectively. The BEs and peak areas were optimized to achieve the best fitting.

Electrochemical Measurements. Linear sweep voltammetry was performed with a potentiostat with digital data acquisition (TEQ, Argentina) or an Autolab (PGSTAT128N). The MBA-Ag-upd substrate (working electrode) was mounted in a conventional three-electrode glass cell using a Pt large area wire as counter and a saturated calomel electrode (SCE) as reference electrodes, respectively. Aqueous 0.1 M NaOH solutions were prepared by using deionized H_2O from a Milli-Q purification system which were degassed with purified nitrogen prior to the experiments.

MBA reductive electrodesorption was performed by scanning the potential from −0.3 to −1.6 at 0.05 V s^{-1} in the 0.1 M NaOH aqueous solution at room temperature. In each case the charge density involved in the reductive desorption (calculated by integration of the peak area and taking into account the electrode real area from the gold oxide reduction peak as 440

dx.doi.org/10.1021/jp409785c | J. Phys. Chem. C XXXX, XXX, XXX−XXX

μC cm^{-2}) was taken as an indication of the SAM surface coverage.[35]

Synthesis of Silver Nanoparticles. Silver nanoparticles (AgNPs) in aqueous solution were prepared by reduction of $AgNO_3$ with $NaBH_4$ and stabilized by using trisodium citrate. All reagents used in the synthesis were of analytical grade, and solutions were prepared with Milli-Q water (18 MΩ cm). Briefly, 10 mL of a 0.25 mM aqueous $AgNO_3$ solution was added to 10 mL of a 0.25 mM aqueous sodium citrate solution under softly magnetic stirring. Then, 25 μL of a freshly prepared 100 mM aqueous $NaBH_4$ solution cooled in an ice/water bath at around 0 °C was added dropwise. The initially colorless solution became yellow and was stirred vigorously for 3 min. The final Ag concentration in the NP solution is 2.1 × 10^{-2} mg Ag/mL. The colloidal suspension was then dialyzed 2 h to eliminate the excess of citrate. Afterward, the dialyzed citrate-capped AgNPs were mixed with a MBA 1 mM + 0.1 M NaOH in a 10:1 ratio (citrate Ag NPs:MBA solution) to replace the weakly adsorbed citrate anions by MBA (ligand exchange). Finally, after 2 h of reaction, the colloidal suspension was again dialyzed for 12 h against 0.01 M NaOH.

TEM Characterization. The MBA-protected AgNPs were characterized by using a FEI CM200 UT microscope operated at 200 keV and a FEI TECNAI F20 field emission operated a 200 keV.

DFT Calculations. The DFT calculations have been performed with the periodic plane-wave basis set code VASP 5.2.12.[36,37] We have followed the scheme of nonlocal functionals proposed by Dion et al.,[38] vdW-DF, and the optimized Becke88 exchange functional optB88-vdW[39] to take into account the van der Waals (vdW) interactions. The electronic wave functions were expanded in a plane-wave basis set with a 450 eV cutoff energy. The projector augmented plane wave (PAW) due to the Blöchl method has been used to represent the atomic cores[40] with PBE potential. Silver surfaces were represented by a five atomic layer slab with ∼12 Å vacuum. Optimal grids of Monkhorst−Pack[41] k-points of 9 × 4 × 1 and 7 × 7 × 1 have been used for numerical integration in the reciprocal space of $(\sqrt{3} \times 4)$ and $(\sqrt{7} \times \sqrt{7})R19.1°$ surface structures, respectively. Surface relaxation is allowed in the three uppermost Ag layers of the slab. MBA radical species were optimized in an asymmetric box of 10 Å × 12 Å × 14 Å. The calculated lattice constant is 4.14 Å, which compares reasonably well with the experimental value (4.09 Å).[42]

The average binding energy per adsorbed MBA* radical, which results when MBA loses the hydrogen atom of the S−H group on Ag(111) surface, E_b, is defined in eq 1:

$$E_b = \frac{1}{N_{MBA*}}[E^{MBA*/Ag} - E^{R}_{Ag(111)} - N_{MBA*}E_{MBA*}] \quad (1)$$

where $E^{MBA*/Ag}$, $E^{R}_{Ag(111)}$, and E_{MBA*} stand for the total energy of the adsorbate−substrate system, the Ag slab when MBA* moieties are removed, and the MBA* radical, respectively, whereas N_{MBA*} is the number of MBA* radicals in the surface unit cell. A negative number indicates that adsorption is exothermic with respect to the separate clean surface and MBA* radical.

RESULTS AND DISCUSSION

Planar Surfaces. *XPS Characterization.* Typical high-resolution XPS spectra of the S 2p for MBA SAMs on Ag-upd and polycrystalline Ag foil formed by immersion for t = 10 min in aqueous 0.1 M NaOH are shown in Figure 1a,b. The S 2p region spectra for the Ag-upd and Ag foil substrates can be

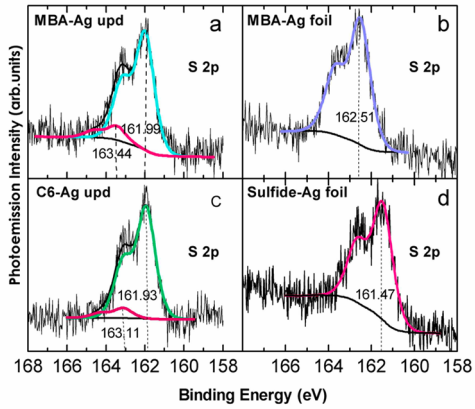

Figure 1. (a) XPS spectra of MBA adsorbed on Ag-upd. (b) XPS spectra of MBA adsorbed on Ag foil. The SAM was obtained by immersion of a 1 mM MBA ethanolic solution for 1 h 30 min. (c) XPS spectra of 1-hexanethiol (C6) adsorbed on Ag-upd. The SAM was obtained by immersion of a 1 mM C6 ethanolic solution for 24 h. (d) XPS spectra of sulfide adsorbed on Ag foil. The S adlayer was obtained by immersion of a 1 mM Na_2S aqueous solution for 5 min.

fitted with a main component at S $2p_{3/2}$ BE ≈ 162 eV, which has been assigned to the formation of a thiolate−Ag bond. In some cases a minor component at ≈163 eV (<10%) is found which can be assigned to physisorbed MBA molecules (Figure 1a). Similar results were obtained for 1-hexanethiol (Figure 1c) and 1-hexadecanethiol (not shown) self-assembled on the Ag-upd surface. We exclude the formation of adsorbed sulfides on the MBA, C6, and C16 SAMs since, when present, they originate a S 2p peak at 161.4 eV as is shown in Figure 1d. These results are consistent with the formation of a SAM of intact thiol molecules adsorbed to the Ag surface by forming strong thiolate−Ag bonds.

We have used the information given by the XPS spectra to estimate the MBA coverage on the Ag-upd surface. The 162 eV S 2p (thiolate)/Ag signal ratio (r) for C6 and C16 is r = 0.30−0.31 while for MBA it results in r = 0.22. Thus, considering that for alkanethiols the high coverage phase is $\theta \approx 0.44$, the surface coverage for MBA should be $\theta \approx 0.3$. This result indicates that MBA forms a more diluted lattice than alkanethiols on the Ag(111) surface.

Electrochemical Data. Electrochemical desorption was carried out by sweeping the potential from an initial value where the chemisorbed layer is stable up to potentials where the adsorbates are removed from the Ag-upd surface. Figure 2a,b shows typical current density (j) vs potential (E) curves recorded in a 0.1 M NaOH aqueous solution after MBA SAM formation in ethanol (Figure 2a) and aqueous 0.1 M NaOH solution (Figure 2b) on Ag-upd for 1 h 30 min. The presence of well-defined peak located at E_p = −1.1 V in the j vs E profiles can be unambiguously assigned to desorption of the adsorbed MBA molecules from the Ag-upd surface, irrespective of the solvent used for self-assembly.

On the other hand, the electrodesorption of C6 and C16 SAMs on Ag upd is shown in Figure 2c,d. The potentials at which these processes occur are placed at more negative potentials than that of MBA SAMs according to higher van der

dx.doi.org/10.1021/jp409785c | J. Phys. Chem. C XXXX, XXX, XXX−XXX

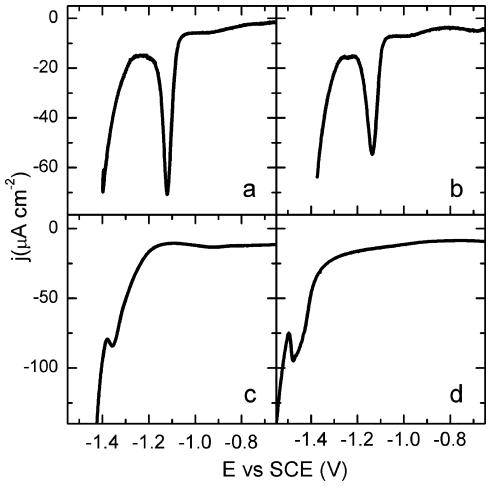

Figure 2. Electrodesorption of MBA SAMs from Ag-upd. (a) SAM self-assembled in 0.1 M NaOH aqueous solution. (b) SAM self-assembled in ethanol. (c) Electrodesorption of 1-hexanethiol SAM self-assembled in ethanol, from Ag-upd. (d) Electrodesorption of 1-hexadecanethiol SAM self-assembled in ethanol, from Ag-upd. Electrolyte: NaOH 0.1 M. The SAMs were obtained by immersion in 1 mM MBA + 0.1 M NaOH for 1 h 30 min and in 1 mM hexanethiol and 1 mM hexadecanethiol ethanolic solutions for 24 h.

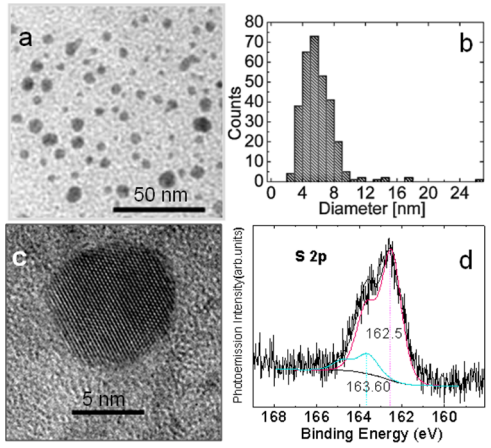

Figure 3. (a) TEM image of freshly prepared MBA-protected AgNPs. (b) Size analysis of a sample of 309 Ag NPs. (c) HRTEM of one MBA-Ag NP. (d) XPS spectra of freshly prepared MBA-protected AgNPs obtained by a ligand-exchange method of citrate-capped Ag NPs.

Waals forces and lower solubility in the aqueous solution used in the electrodesorption process.[43] The charge density (q) obtained from these desorption curves gives also an estimation of the thiol surface coverage. In the case of MBA we found q = 55 ± 7 μC cm^{-2} irrespective of the immersion time. On the other hand, the estimation of the surface coverage for the C6 and C16 SAMs is more difficult due to the partial superposition with the hydrogen evolution reaction (Figure 2c,d). However, after deconvolution of these peaks from the hydrogen evolution reaction the charge estimation results in $q \cong 100$ μC cm^{-2}. This value is consistent with the presence of a densely packed monolayer in a $(\sqrt{7} \times \sqrt{7})R19.1°$ arrangement (surface coverage θ = 0.44) and the desorption reaction

$$RS{-}Ag + e^- = RS^- + Ag \quad (2)$$

Therefore, the value q = 55 ± 7 μC cm^{-2} can hardly be assigned to a MBA monolayer in a $(\sqrt{7} \times \sqrt{7})R19.1°$ lattice like that found for alkanethiols on Ag(111). Taking into account the q values reported for alkanethiols and MBA, we can estimate $\theta \approx 0.25 \pm 0.02$, i.e., close to $\theta \approx 0.3$ estimated from the XPS data. The value $\theta \approx 0.25$ resulting from the electrochemical measurements is that expected for a $(\sqrt{3} \times 4)$ lattice found for MBA on Au(111) by scanning tunneling microscopy (STM).[44] Interestingly, longer immersion times (12−24 h) did not change electrochemical results; i.e., the surface coverage remains constant at least in the time range of our experiments.

AgNPs. A typical TEM image of freshly MBA-protected AgNPs is shown in Figure 3a. The histogram shows that the average size of the MBA-protected AgNPs is 6 ± 3 nm (Figure 3b). HRTEM allows resolving the atomic structure of the AgNP (Figure 3c). The image is compatible with a [110] zone axis of an fcc structure like Ag. Moreover, the presence of this and other planes evidences the crystallinity of the nanoparticles. XPS data of these AgNPs are shown in Figure 3d. The S 2p signal exhibits, in agreement with that observed for MBA on Ag-upd (Figure 1), the main component at ≈162 eV (84.5%) and the minor one at ≈163 eV (13.5%) assigned to thiolates and physisorbed MBA molecules, respectively. However, we found that the 162 eV S 2p/Ag ratio is r = 0.50, whereas for planar Ag-upd surfaces it is r = 0.22. This is not an unexpected value since the coverage of thiolates on metallic NPs is higher than that found on planar surfaces.[45] For AgNPs smaller than 5 nm in diameter, a great number of Ag atoms are located at corners and edges of the surface. In this way the high radius of curvature of the NPs allows a larger proportion of the Ag atoms to be on the surface, which in turn results in a greater coverage of the thiol-adsorbed monolayer as was found previously for AuNPs.[45] Modeling of AuNPs has shown that the coverage is about twice that expected for the Au(111) surface.[46] In our case the measured 162 eV S 2p/Ag ratio is r = 0.50, a figure between $2r$ = 0.44 and $2r$ = 0.6 measured for MBA (θ = 0.25) and alkanethiolates (θ = 0.44) on the Ag upd surface (Figure 1), respectively. Finally, in contrast to that observed for other thiolate-protected AgNPs,[22,23] no evidence of sulfides (161.4 eV S 2p component) has been found in the spectra (Figure 3d), in agreement with that observed for MBA on the Ag upd surface. In principle, this difference could result from the different synthetic methods used to prepare the thiolate-protected AgNPs. However, XPS data for dodecanethiolate-protected AgNPs synthesized by the two-phase Brust−Schiffrin method in our laboratory showed only a small amount of sulfide, which is not consistent with thiolates grafted on Ag@Ag_2S core@shell model.[16] Also, thermogravimetric analysis data for thiolate-protected AgNPs prepared by the one-phase Brust−Schiffrin method showed no evidence of an excess of S in relation to that intact thiolate species.[47] However, it has been shown that thiolate-protected AgNPs and thiolate-protected Ag@Ag_2S core@shell NPs have a similar stability,[16] so that the final product could depend on details of the synthetic procedure or by the presence of sulfide impurities.

Typical TEM image of the MBA-protected AgNPs after 2 week aging is shown in Figure 4a. The particle size histogram of the aged MBA-protected AgNPs shows two distributions for NPs sizes: one around 6 ± 2 nm and the other at 15 ± 3 nm (Figure 4b); i.e., the aging process results in AgNP sintering. HRTEM allows resolving the atomic structure of the aged AgNP (Figure 4c,e). The indexation of the pattern is

dx.doi.org/10.1021/jp409785c | J. Phys. Chem. C XXXX, XXX, XXX−XXX

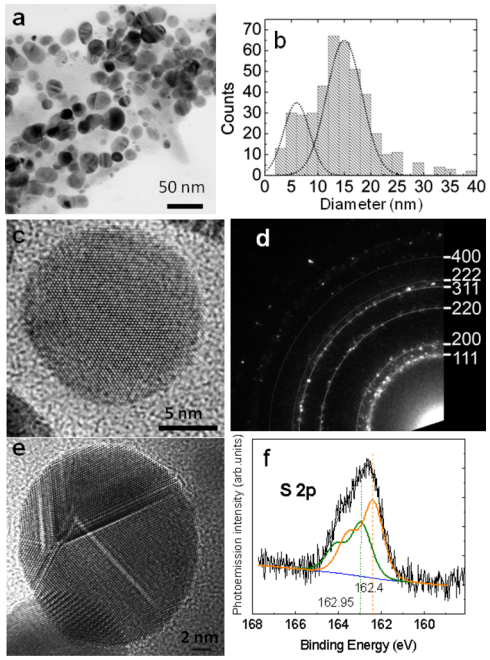

Figure 4. (a) Bright field image of aged (for 2 weeks) MBA-Ag NPs. (b) Size analysis of a sample of 422 AgNPs. (c, e) HRTEM images of individual MBA-protected AgNP. (d) ED pattern of MBA-protected AgNPs revealing only the Ag crystalline planes. (f) XPS spectra of 15 days aged MBA-protected AgNPs.

compatible with the fcc structure of Ag (Figure 4d) and confirms the absence of Ag_2S. Faults and twin boundaries shown in Figure 4e are compatible with the presence of faceted particles.[48] The S 2p data for the aged AgNPs (Figure 4f) show that the total amount of S slightly decreases with respect to that measured for the freshly prepared AgNPs (Figure 3d). More importantly, we note that the 162 eV component (60%) decreases and the 163 eV component increases (40%) (Figure 4e). Similar behavior has been reported during the aging of nanostructured Au surfaces where the increase in the 163 eV component was assigned to disulfide formation resulting from the oxidation of thiolates.[35] The degradation of the protective MBA layer explains the sintering process and, therefore, the increase in the AgNP size from 6 to 15 nm. More important is that these data show that sintering takes places even with a small degradation of the thiolate layer.

Figure 5a shows a typical MBA-protected AgNP where five [110] fcc zone axis rotated 72° of each other could be observed, and the corresponding FFT is shown in the inset. The existence

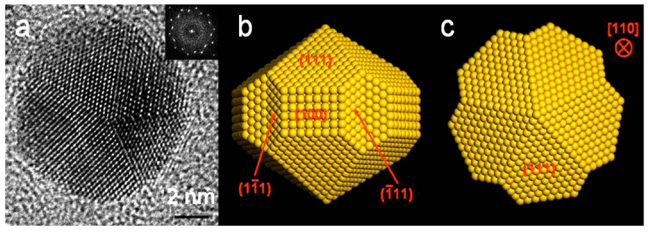

Figure 5. (a) HRTEM of a MBA-protected AgNP. The image is consistent with a Marks decahedron at [110] projection (the inset is the FFT pattern). (b) Marks decahedron model from [100] fcc. (c) Marks decahedron model from [110] fcc. All faces are labeled according to a fcc structure.

of 5-fold symmetry in fcc structures was already explained by Bagley[49] as a 5-fold twin ((111) twinning plane) with five face-centered cubic individual crystals about a common [110] axis. Different views of a Marks' decahedron model with their faces labeled according to Ag structure are shown in Figure 5b,c. This model interprets the HRTEM image of Figure 5a and allows to see the preponderant contribution of the (111) and (100) faces on the surface area. Theoretical calculations have shown that this shape is the most stable for AgNPs at intermediate sizes.[50]

DFT Results. DFT calculations have been employed to explore the energetic and structural characteristics of different models for MBA adsorption on Ag(111) and Ag(100) since these planes are relevant on the AgNPs. Following our previous work about the MBA SAMs on Au(111), we have first studied the adsorption on an unreconstructed (U) Ag(111) surface modeled by a $(\sqrt{3} \times 4)$ unit cell with two MBA radicals oriented along the $[11\bar{2}]$ and $[1\bar{2}1]$ directions, with θ_{MBA} = 0.25. The optimized surface structure is shown in Figure 6a.

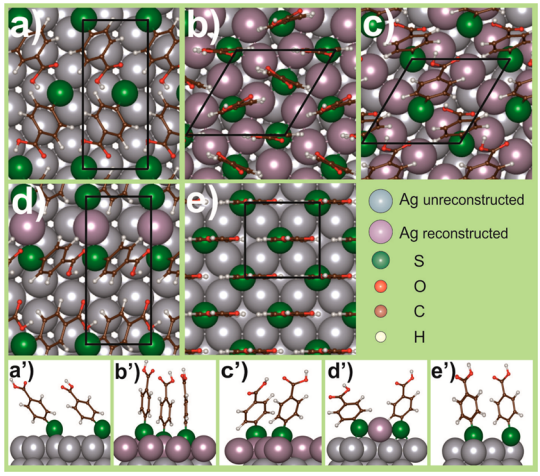

Figure 6. Optimized structures for MBA* on Ag(111) and Ag(100) metal surfaces: (a) $(\sqrt{3} \times 4)$, (b) $(R7_{3/7})$, (c) $(R7_{2/7})$, (d) $(\sqrt{3} \times 4)$ with RS−Ag−SR species, and (e) c(2 × 2). Surface unit cells are indicated by a black line. a′, b′, c′, d′, and e′ correspond to the lateral views of the surface models shown in a, b, c, d, and e, respectively.

The preferential adsorption sites for this model involve MBA* species in standing-up configuration with the S atoms located either on bridge-fcc hollow or on bridge-hcp hollow sites. The molecular axis of the adsorbed MBA* is tilted 47.3° (bridge-hcp) and 44.2° (bridge-fcc) with respect to the surface normal (Figure 6a′). Distances between nearest-neighbor MBA radicals are 0.51 and 0.60−0.65 nm. Attempts made to optimize this surface structure decreasing the tilt angle resulted in lower binding energies, suggesting that attractive interactions between the aromatic ring and the Ag surface are important for this molecular arrangement.

The second surface structure (Figure 6b) studied here consists of a $(\sqrt{7} \times \sqrt{7})R19.1°$ MBA* lattice on a reconstructed (R) Ag(111) surface with 5/7 of Ag atoms in the outmost layer and θ_{MBA}= 3/7 $(R7_{3/7})$ that has been already proposed for thiol-protected Ag(111)[11] and nanoclusters.[51] In this model the three MBA* adsorb in bridge sites between Ag overlayer atoms with a standing-up configuration and the molecular axis tilted by 3.6°−6.6° (Figure 6b′). The calculated S−S distance is 0.42−0.47 nm. We have also analyzed the same $(\sqrt{7} \times \sqrt{7})R19.1°$ surface structure but in this case with θ_{MBA}

dx.doi.org/10.1021/jp409785c | J. Phys. Chem. C XXXX, XXX, XXX−XXX

Table 1. Energetic, Coverage, and Bader Charge from DFT Calculations for MBA Adsorption on Ag(111) (Reconstructed and Unreconstructed) and Ag(100)

surface lattice	$(\sqrt{3} \times 4)$	$(\sqrt{3} \times 4)$	$(\sqrt{7} \times \sqrt{7})R19.1°$	$(\sqrt{7} \times \sqrt{7})R19.1°$	c(2 × 2)
metal surface	Ag(111) U	Ag(111) R	Ag(111) R	Ag(111) R	Ag(100) U
θ_{MBA}	1/4	1/4	2/7	3/7	1/2
E_b/eV	−2.73	−2.99	−3.29	−2.59	−2.66
E_{rec}/N_{thiol}/eV	0.0	+0.34	+0.76	+0.52	0.0
$E_b + E_{rec}/N_{thiol}$/eV	−2.73	−2.65	−2.53	−2.07	−2.66
q(S)/e	−0.30	−0.28	−0.29	−0.30	−0.34
q(Ag)/e	+0.07	+0.31,[a] +0.03	+0.14	+0.22	+0.17

[a]Ag adatom.

= 2/7 ($R7_{2/7}$) (Figure 6c) since it is close to the experimental coverage θ_{MBA} = 0.25/0.30. In this model both MBA* adsorb on a bridge configuration between the Ag overlayer atoms. The MBA* species are placed in a standing-up configuration with the molecular axis tilted 22.8° (2-Ag-coordinated MBA*) and 40° (3-Ag-coordinated MBA*) with respect to the surface normal (Figure 6c′). The calculated distances between nearest-neighbor MBA radicals are 0.41 and 0.53 nm. We have also tested several MBA* adsorption sites for both $R7_{3/7}$ and $R7_{2/7}$ models, and the data presented herein are the most stable ones for both configurations. We have also considered a $(\sqrt{3} \times 4)$ lattice but formed by RS-Ag-RS complexes following the model for thiolates on the Au(111) surface[19,52,53] (Figure 6d). We observe that the Ag adatom in the optimized structure is placed at the hcp hollow rather than at the bridge site observed for the RS−Au−RS moieties on the Au(111) surface. Thus, the S atoms are also bound to Ag atoms at the bridge sites of the Ag surface. The S−Ag−S angle in the staple is 176°. On the other hand, the tilt angles of the MBA* moieties in the staple are 53.8° and 33.6°, respectively (Figure 6d′).

Finally, the MBA* radicals adsorbed on the Ag(100) surface in a c(2 × 2) unit cell with two MBA* moieties per unit cell and θ_{MBA} = 1/2 (Figure 6e). This model is also important since as shown in Figures 4 and 5 the AgNPs with sizes larger than 5 nm consist of (111) and (100) faces.[50] In this case the hollow positions are the most stable sites for MBA*, and the tilt angle is ≈0° (Figure 6e′).

A summary of the structural and energetic parameters obtained for the optimized configurations of the models shown in Figure 6 is presented in Table 1.

These data reveal that the largest E_b value is found for the $R7_{2/7}$ model. We also observe that the strength of the adsorption process decreases with the increase in the MBA* surface coverage in going from the $R7_{2/7}$ to $R7_{3/7}$.

A Bader charge analysis of the optimized configurations is also presented in Table 1. The charge transfer from the Ag surface to the MBA* species results in negatively charged S atoms in the MBA* moieties and positively charged Ag atoms. The analysis of the Bader charge also shows that the Ag−S thiolate bond is more ionic than the S−Au bond in MBA SAMs on Au(111).[44]

Results also show the stability of the MBA* adsorbate in terms of the balance between the binding energy (E_b) plus the energy to reconstruct the Ag surface (E_{rec}) given by ($E_b + E_{rec}/N_{MBA*}$) with $E_{rec} = E^{R}_{Ag(111)} - (E^{U}_{Ag(111)} - n_{vac}E^{Ag}_{bulk})$, where $E^{R}_{Ag(111)}$ and $E^{U}_{Ag(111)}$ correspond to the energy of reconstructed Ag(111) and unreconstructed Ag(111) surface, respectively, E^{Ag}_{bulk} is the total energy of the bulk Ag atom, and n_{vac} is the number of Ag vacancies in the surface unit cell. Data in Table 1 show that the $(\sqrt{3} \times 4)$ model on the unreconstructed surface presents the best stability as this model do not involve any cost to form Ag vacancies on the Ag(111) surface. In contrast, the $(\sqrt{3} \times 4)$ lattice consisting of RS−Ag−RS moieties (Figure 6d) is less stable (Table 1) due to the energy needed to extract the Ag adatom from the Ag(111) surface. It is also interesting the high stability exhibited by the MBA SAM on the Ag(100) surface.

Now we analyze the possibility of a transition from the diluted $(\sqrt{3} \times 4)$ MBA lattice to the denser $R7_{3/7}$ and $R7_{2/7}$ surfaces already proposed for alkanethiol SAMs on Ag(111)[9,11] by using the Gibbs free energy of adsorption ($\gamma(\Delta\mu)$) defined as

$$\gamma(\Delta\mu_{MBA*}) \approx \frac{1}{A}[E^{MBA*/Ag} - N_{Ag}E^{bulk}_{Ag} - N_{MBA*}\Delta\mu_{MBA*}] - \gamma^{U}_{clean}$$
$$\approx \frac{N_{MBA*}}{A}\left[E^{(MBA)_2}_{b} + \frac{E_{rec}}{N_{MBA*}}\right] + \gamma^{U}_{clean} - \frac{N_{MBA*}}{A}\Delta\mu_{MBA*} \quad (3)$$

as a function of the chemical potential ($\Delta\mu_{MBA*}$), where $E_b^{(MBA)_2}$ represents the binding energy per MBA* calculated with respect the total energy of gas phase $(MBA)_2$, A is the area of the surface unit cell, and γ^{U}_{clean} is the Gibbs free energy of the unreconstructed Ag(111) surface. The phase diagram (Figure 7) clearly shows that for $\Delta\mu_{MBA*} > -1.5$ eV the diluted $(\sqrt{3} \times 4)$ becomes thermodynamically more stable than the clean Ag(111) surface. Besides, the $(\sqrt{3} \times 4)$ results more stable than the $R7_{2/7}$ and $R7_{3/7}$ lattices in the overall $\Delta\mu_{MBA*}$ studied in this work.

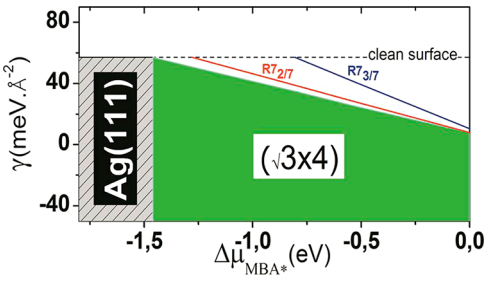

Figure 7. γ vs $\Delta\mu_{MBA}$ plots for the $(\sqrt{3} \times 4)$, $R7_{2/7}$, and $R7_{3/7}$ lattices.

CONCLUSIONS

We have made a comparative study of MBA on Ag (111) and AgNPs. We have found that MBA adsorbs intact as thiolate on the Ag surface without formation of silver sulfide. MBA forms a diluted and stable surface structure on the Ag (111) faces with a surface coverage smaller than that found for alkanethiolates. On the other hand, DFT calculations suggest larger thiol coverage and unreconstructed surfaces after thiol adsorption on the

dx.doi.org/10.1021/jp409785c | J. Phys. Chem. C XXXX, XXX, XXX−XXX

(100) Ag faces. In agreement with that observed for thiol-protected AuNPs, the MBA layer is denser on the AgNP surfaces due to curvature effects. Slow degradation of the protective MBA layer takes place on the AgNPs, leading to thiolate transformation to the corresponding disulfide. This process leads to NP sintering even for a small amount of thiolate degradation.

■ ASSOCIATED CONTENT

Supporting Information

The upd Ag on Au voltammogram (Figure S1) and HRTEM images with FFTs of MBA-protected AgNPs (Figure S2). This material is available free of charge via the Internet at http://pubs.acs.org.

■ AUTHOR INFORMATION

Corresponding Author

*E-mail mevela@inifta.unlp.edu.ar; Ph +54 221 4257430; Fax +54 221 4254642 (M.E.V.).

Notes

The authors declare no competing financial interest.

■ ACKNOWLEDGMENTS

We acknowledge financial support from ANPCyT (PICT 2010-2554 and CTQ2011-24784), MICINN, Spain. P.C. thankfully acknowledges the computer resources provided by the Computer Support Service for Research (SAII) at La Laguna University. M.E.V. is a researcher from CIC BsAs.

■ REFERENCES

(1) Gates, B. D.; Xu, Q.; Stewart, M.; Ryan, D.; Willson, C. G.; Whitesides, G. M. New Approaches to Nanofabrication: Molding, Printing, and Other Techniques. *Chem. Rev.* **2005**, *105*, 1171−1196.

(2) Kind, M.; Wöll, C. Organic Surfaces Exposed by Self-Assembled Organothiol Monolayers: Preparation, Characterization, and Application. *Prog. Surf. Sci.* **2009**, *84*, 230−278.

(3) Love, J. C.; Estroff, L. A.; Kriebel, J. K.; Nuzzo, R. G.; Whitesides, G. M. Self-Assembled Monolayers of Thiolates on Metals as a Form of Nanotechnology. *Chem. Rev.* **2005**, *105*, 1103−1169.

(4) Vericat, C.; Vela, M. E.; Benitez, G.; Carro, P.; Salvarezza, R. C. Self-Assembled Monolayers of Thiols and Dithiols on Gold: New Challenges for a Well-Known System. *Chem. Soc. Rev.* **2010**, *39*, 1805−1834.

(5) Vericat, C.; Vela, M. E.; Salvarezza, R. C. Self-Assembled Monolayers of Alkanethiols on Au(111): Surface Structures, Defects and Dynamics. *Phys. Chem. Chem. Phys.* **2005**, *7*, 3258−3268.

(6) Laibinis, P. E.; Whitesides, G. M.; Allara, D. L.; Tao, Y. T.; Parikh, A. N.; Nuzzo, R. G. Comparison of the Structures and Wetting Properties of Self-Assembled Monolayers of n-Alkanethiols on the Coinage Metal Surfaces, Copper, Silver and Gold. *J. Am. Chem. Soc.* **1991**, *113*, 7152−7167.

(7) Rong, H. T.; Frey, S.; Yang, Y. J.; Zharnikov, M.; Buck, M.; Wühn, M.; Wöll, C.; Helmchen, G. On the Importance of theHheadgroup Substrate Bond in Thiol Monolayers: A Study of Biphenyl-based Thiols on Gold and Silver. *Langmuir* **2001**, *17*, 1582−1593.

(8) Yu, M.; Woodruff, D. P.; Satterley, C. J.; Jones, R. G.; Dhanak, V. R. Structure of the Pentylthiolate Self-Assembled Monolayer on Ag(111). *J. Phys. Chem. C* **2007**, *111*, 10040−10048.

(9) Yu, M.; Driver, S. M.; Woodruff, D. P. Scanning Tunneling Microscopy Investigation of the Structure of Methanethiolate on Ag(111). *Langmuir* **2005**, *21*, 7285−7291.

(10) Torres, D.; Carro, P.; Salvarezza, R. C.; Illas, F. Evidence for the Formation of Different Energetically Similar Atomic Structures in Ag(111)-($\sqrt{7}$x$\sqrt{7}$)-R19.1°-CH_3S. *Phys. Rev. Lett.* **2006**, *97*, 226103.

(11) Abufager, P. N.; Alvarez Soria, L.; Martiarena, M. L.; Reuter, K.; Busnengo, H. F. Structure of the Methylthiolate Monolayer on Ag (111): The Role of Substrate Vacancies. *Chem. Phys. Lett.* **2011**, *503*, 71−74.

(12) Fenter, P.; Eisenberger, P.; Li, J.; Camillone, N.; Bernasek, S.; Scoles, G.; Ramanarayanan, T. A.; Liang, K. S. Structure of Octadecyl Thiol Self-Assembled on the Silver(111) Surface: an Incommensurate Monolayer. *Langmuir* **1991**, *7*, 2013−2016.

(13) Hu, L.; de la Rama, L. P.; Efremov, M. Y.; Anahory, Y.; Schiettekatte, F.; Allen, L. H. Synthesis and Characterization of Single-Layer Silver-Decanethiolate Lamellar Crystals. *J. Am. Chem. Soc.* **2011**, *133*, 4367−4376.

(14) Rodríguez, L. M.; Gayone, J. E.; Sánchez, E. A.; Grizzi, O.; Blum, B.; Salvarezza, R. C. Room-Temperature Kinetics of Short-Chain Alkanethiol Film Growth on Ag(111) from the Vapor Phase. *J. Phys. Chem. B* **2006**, *110*, 7095−7097.

(15) Lewis, M.; Tarlov, M.; Carron, K. Study of the Photooxidation Process of Self-Assembled Alkanethiol Monolayers. *J. Am. Chem. Soc.* **1995**, *117*, 9574−9575.

(16) Azcárate, J. C.; Corthey, G.; Pensa, E.; Vericat, C.; Fonticelli, M. H.; Salvarezza, R. C.; Carro, P. Understanding the Surface Chemistry of Thiolate-Protected Metallic Nanoparticles. *J. Phys. Chem. Lett.* **2013**, *4*, 3127−3138.

(17) Chakraborty, I.; Govindarajan, A.; Erusappan, J.; Ghosh, A.; Pradeep, T.; Yoon, B.; Whetten, R. L.; Landman, U. The Superstable 25 kDa Monolayer Protected Silver Nanoparticle: Measurements and Interpretation as an Icosahedral $Ag_{152}(SCH_2CH_2Ph)_{60}$ Cluster. *Nano Lett.* **2012**, *12*, 5861−5866.

(18) Xiang, H.; Wei, S.-H.; Gong, X. Structures of $[Ag_7(SR)_4]^-$ and $[Ag_7(DMSA)_4]^-$. *J. Am. Chem. Soc.* **2010**, *132*, 7355−7360.

(19) Jadzinsky, P. D.; Calero, G.; Ackerson, C. J.; Bushnell, D. A.; Kornberg, R. D. Structure of a Thiol Monolayer-Protected Gold Nanoparticle at 1.1 Å Resolution. *Science* **2007**, *318*, 430−433.

(20) Desireddy, A.; Conn, B. E.; Guo, J.; Yoon, B.; Barnett, R. N.; Monahan, B. M.; Kirschbaum, K.; Griffith, W. P.; Whetten, R. L.; Landman, U.; et al. Ultrastable Silver Nanoparticles. *Nature* **2013**, *501*, 399−402.

(21) Yang, H.; Wang, Y.; Huang, H.; Gell, L.; Lehtovaara, L.; Malola, S.; Häkkinen, H.; Zheng, N. All-thiol-stabilized Ag_{44} and $Au_{12}Ag_{32}$ Nanoparticles with Single-Crystal Structures. *Nat. Commun.* **2013**, *4*, 2422.

(22) Padmos, J. D.; Zhang, P. Surface Structure of Organosulfur Stabilized Silver Nanoparticles Studied with X-ray Absorption Spectroscopy. *J. Phys. Chem. C* **2012**, *116*, 23094−23101.

(23) Battocchio, C.; Meneghini, C.; Fratoddi, I.; Venditti, I.; Russo, M. V.; Aquilanti, G.; Maurizio, C.; Bondino, F.; Matassa, R.; Rossi, M.; et al. Silver Nanoparticles Stabilized with Thiols: A Close Look at the Local Chemistry and Chemical Structure. *J. Phys. Chem. C* **2012**, *116*, 19571−19578.

(24) Corthey, G.; Rubert, A. A.; Picone, A. L.; Casillas, G.; Giovanetti, L. J.; Ramallo-López, J. M.; Zelaya, E.; Benitez, G. A.; Requejo, F. G.; José-Yacamán, M.; et al. New Insights into the Chemistry of Thiolate-Protected Palladium Nanoparticles. *J. Phys. Chem. C* **2012**, *116*, 9830−9837.

(25) Holmlin, R. E.; Ismagilov, R. F.; Haag, R.; Mujica, V.; Ratner, M. A.; Rampi, M. A.; Whitesides, G. M. Correlating Electron Transport and Molecular Structure in Organic Thin Films. *Angew. Chem., Int. Ed.* **2001**, *40*, 2316−2320.

(26) Hong, J.-P.; Park, A.-Y.; Lee, S.; Kang, J.; Shin, N.; Yoon, D. Y. Tuning of Ag Work Functions by Self-Assembled Monolayers of Aromatic Thiols for an Efficient Hole Injection for Solution Processed Triisopropylsilylethynyl Pentacene Organic Thin Film Transistors. *Appl. Phys. Lett.* **2008**, *92*, 143311−3.

(27) Bishnoi, S. W.; Rozell, C. J.; Levin, C. S.; Gheith, M. K.; Johnson, B. R.; Johnson, D. H.; Halas, N. J. All-Optical Nanoscale pH Meter. *Nano Lett.* **2006**, *6*, 1687−1692.

(28) Kneipp, J.; Kneipp, H.; Wittig, B.; Kneipp, K. Following the Dynamics of pH in Endosomes of Live Cells with SERS Nanosensors. *J. Phys. Chem. C* **2010**, *114*, 7421−7426.

(29) Kang, J. F.; Ulman, A.; Liao, S.; Jordan, R.; Yang, G.; Liu, G.-y. Self-Assembled Rigid Monolayers of 4′-Substituted-4-mercaptobiphenyls on Gold and Silver Surfaces. *Langmuir* **2000**, *17*, 95−106.
(30) Pradeep, T.; Evans, C.; Shen, J.; Cooks, R. G. Adsorbate Geometry Distinction in Arenethiols by Ion/Surface Reactive Collisions. *J. Phys. Chem. B* **1999**, *103*, 5304−5310.
(31) Petri, M.; Kolb, D. M.; Memmert, U.; Meyer, H. Adsorption of Mercaptopropionic Acid onto Au(1 1 1): Part I. Adlayer Formation, Structure and Electrochemistry. *Electrochim. Acta* **2003**, *49*, 175−182.
(32) Freire, R. S.; Kubota, L. T. Application of Self-Assembled Monolayer-Based Electrode for Voltammetric Determination of Copper. *Electrochim. Acta* **2004**, *49*, 3795−3800.
(33) Shekhah, O.; Wang, H.; Kowarik, S.; Schreiber, F.; Paulus, M.; Tolan, M.; Sternemann, C.; Evers, F.; Zacher, D.; Fischer, R. A.; et al. Step-by-Step Route for the Synthesis of Metallic Organic Frameworks. *J. Am. Chem. Soc.* **2007**, *129*, 15118−15119.
(34) Urcuyo, R.; Cortés, E.; Rubert, A. A.; Benitez, G.; Montero, M. L.; Tognalli, N. G.; Fainstein, A.; Vela, M. E.; Salvarezza, R. C. Aromatic and Aliphatic Thiol Self-Assembled Monolayers on Au: Anchoring and Delivering Copper Species. *J. Phys. Chem. C* **2011**, *115*, 24707−24717.
(35) Cortés, E.; Rubert, A. A.; Benitez, G.; Carro, P.; Vela, M. E.; Salvarezza, R. C. Enhanced Stability of Thiolate Self-Assembled Monolayers (SAMs) on Nanostructured Gold Substrates. *Langmuir* **2009**, *25*, 5661−5666.
(36) Kresse, G.; Hafner, J. Ab-Initio Molecular-Dynamics for Open-Shell Transition-Metals. *Phys. Rev. B* **1993**, *48*, 13115−13118.
(37) Kresse, G.; Furthmüller, J. Efficiency of ab-Initio Total Energy Calculations for Metals and Semiconductors Using a Plane-Wave Basis Set. *Comput. Mater. Sci.* **1996**, *6*, 15−50.
(38) Dion, M.; Rydberg, H.; Schroder, E.; Langreth, D. C.; Lundqvist, B. I. Van der Waals Density Functional for General Geometries. *Phys. Rev. Lett.* **2004**, *92*, 246401.
(39) Klimes, J.; Bowler, D. R.; Michaelides, A. A Critical Assessment of Theoretical Methods for Finding Reaction Pathways and Transition States of Surface Processes. *J. Phys.: Condens. Matter* **2010**, *22*, 074203−074203.
(40) Blöchl, P. E. Projector Augmented-Wave Method. *Phys. Rev. B* **1994**, *50*, 17953−17979.
(41) Monkhorst, H. J.; Pack, J. D. Special Points for Brillouin-Zone Integrations. *Phys. Rev. B* **1976**, *13*, 5188−5192.
(42) Pearson, W. B. *Handbook of Lattice Spacing and Structure of Metals*; Pergamon Press, Inc.: New York, 1958.
(43) Azzaroni, O.; Vela, M. E.; Andreasen, G.; Carro, P.; Salvarezza, R. C. Electrodesorption Potentials of Self-Assembled Alkanethiolate Monolayers on Ag(111) and Au(111). An Electrochemical, Scanning Tunneling Microscopy and Density Functional Theory Study. *J. Phys. Chem. B* **2002**, *106*, 12267−12273.
(44) Pensa, E.; Rubert, A. A.; Benitez, G.; Carro, P.; Orive, A. G.; Creus, A. H.; Salvarezza, R. C.; Vericat, C. Are 4-Mercaptobenzoic Acid Self Assembled Monolayers on Au(111) a Suitable System to Test Adatom Models? *J. Phys. Chem. C* **2012**, *116*, 25765−25771.
(45) Vericat, C.; Benitez, G. A.; Grumelli, D. E.; Vela, M. E.; Salvarezza, R. C. Thiol-Capped Gold: from Planar to Irregular Surfaces. *J. Phys.: Condens. Matter* **2008**, *20*, 184004.
(46) Luedtke, W. D.; Landman, U. Structure and Thermodynamics of Self-Assembled Monolayers on Gold Nanocrystallites. *J. Phys. Chem. B* **1998**, *102*, 6566−6572.
(47) Farrag, M.; Thämer, M.; Tschurl, M.; Bürgi, T.; Heiz, U. Preparation and Spectroscopic Properties of Monolayer-Protected Silver Nanoclusters. *J. Phys. Chem. C* **2012**, *116*, 8034−8043.
(48) Ling, T.; Xie, L.; Zhu, J.; Yu, H.; Ye, H.; Yu, R.; Cheng, Z.; Liu, L.; Yang, G.; Cheng, Z.; et al. Icosahedral Face-Centered Cubic Fe Nanoparticles: Facile Synthesis and Characterization with Aberration-Corrected TEM. *Nano Lett.* **2009**, *9*, 1572−1576.
(49) Bagley, B. G.; Dense, A. Packing of Hard Spheres with Five-fold Symmetry. *Nature* **1965**, *208*, 674−675.
(50) Wang, B.; Liu, M.; Wang, Y.; Chen, X. Structures and Energetics of Silver and Gold Nanoparticles. *J. Phys. Chem. C* **2011**, *115*, 11374−11381.
(51) Abufager, P. N.; Solano Canchaya, J. G.; Wang, Y.; Alcamí, M.; Martín, F.; Alvarez Soria, L.; Martiarena, M. L.; Reuter, K.; Busnengo, H. F. Theoretical Study of the Structure of Self-Assembled Monolayers of Short Alkylthiolates on Au(111) and Ag(111): The Role of Induced Substrate Reconstruction and Chain-chain Interactions. *Phys. Chem. Chem. Phys.* **2011**, *13*, 9353−9362.
(52) Voznyy, O.; Dubowski, J. J.; Yates, J. T., Jr.; Maksymovych, P. The Role of Gold Adatoms and Stereochemistry in Self-Assembly of Methylthiolate on Au(111). *J. Am. Chem. Soc.* **2009**, *131*, 12989−12993.
(53) Maksymovych, P.; Voznyy, O.; Dougherty, D. B.; Sorescu, D. C.; Yates, J. T., Jr. Gold Adatom as a Key Structural Component in Self-Assembled Monolayers of Organosulfur Molecules on Au(111). *Prog. Surf. Sci.* **2010**, *85*, 206−240.